A Flexible Dual-mode Sensor with Decoupled Strain and Temperature Sensing for Smart Robots

Shiying Li, Mengyu Yang, Yuanzhao Wu,* Waqas Asghar, Xingjian Lu, Haifeng Zhang, Enhong Cui, Zaojun Fang, Jie Shang, Yiwei Liu* and Run-Wei Li*

S. Li, M. Yang, X. Lu, H. Zhang, Y. Wu*, W. Asghar, Prof. J. Shang, Prof. Y. Liu*, Prof. R.-W. Li*
CAS Key Laboratory of Magnetic Materials and Devices, Ningbo Institute of Materials Technology and Engineering, Chinese Academy of Sciences, Ningbo, 315201, P. R. China
wuyz@nimte.ac.cn (Dr. Y. Wu); liuyw@nimte.ac.cn (Prof. Y. Liu); runweili@nimte.ac.cn (Prof. R.-W. Li)

S. Li, M. Yang, X. Lu, H. Z, Y. Wu*, W. Asghar, Prof. J. Shang, Prof. Y. Liu*, Prof. R.-W. Li*
Zhejiang Province Key Laboratory of Magnetic Materials and Application Technology, Ningbo Institute of Materials Technology and Engineering, Chinese Academy of Sciences, Ningbo, 315201, P. R. China.

Prof. R.-W. Li*
School of Future Technology, University of Chinese Academy of Sciences, Beijing 100049, China

Prof. R.-W. Li*
Center of Materials Science and Optoelectronics Engineering, University of Chinese Academy of Sciences, Beijing 100049, China

W. Asghar
Mechanical Engineering Department, University of Engineering and Technology Taxila, 47050, Taxila, Pakistan

Enhong Cui
Shandong Aluminum Valley Testing Center，Shandong Aluminum Valley Industrial Technology Institute, Bingzhou, 256200, P. R. China.

Zaojun Fang
Zhejiang Key Laboratory of Robots and Intelligent Manufacturing Equipment Technology, Ningbo Institute of Materials Technology and Engineering, Chinese Academy of Sciences, Ningbo, 315201, P. R. China.

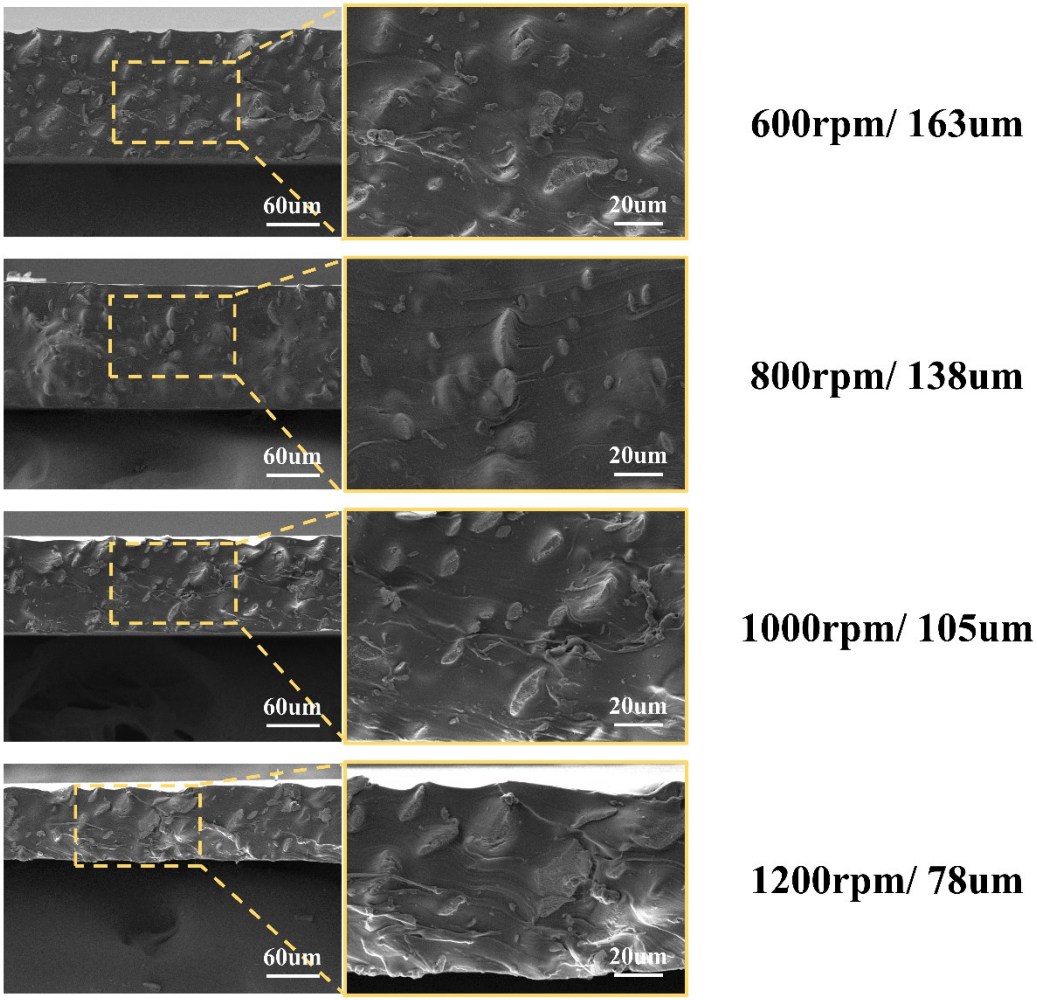

Figure S1 SEM images showing the TSL's thickness (163, 138, 105 and 78 μm), obtained by adjusting spin-coating speeds at 600, 800, 1000, and 1200 rpm, respectively.

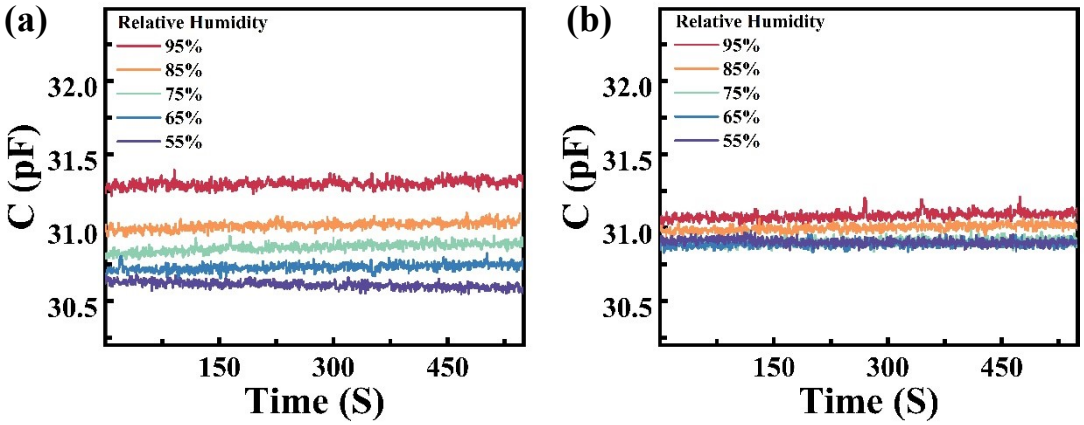

Figure S2 Effect of humidity on temperature detection. (a) Capacitance value of unpackaged device at different levels of humidity and 30 ℃. (b) Capacitance value of packaged device at different levels of humidity and 30 ℃.

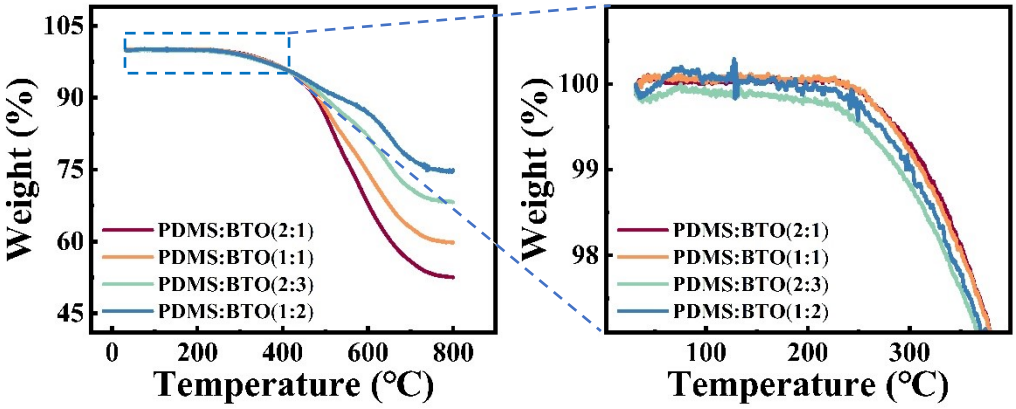

Figure S3 Thermogravimetric analysis of TSL at various mass ratio

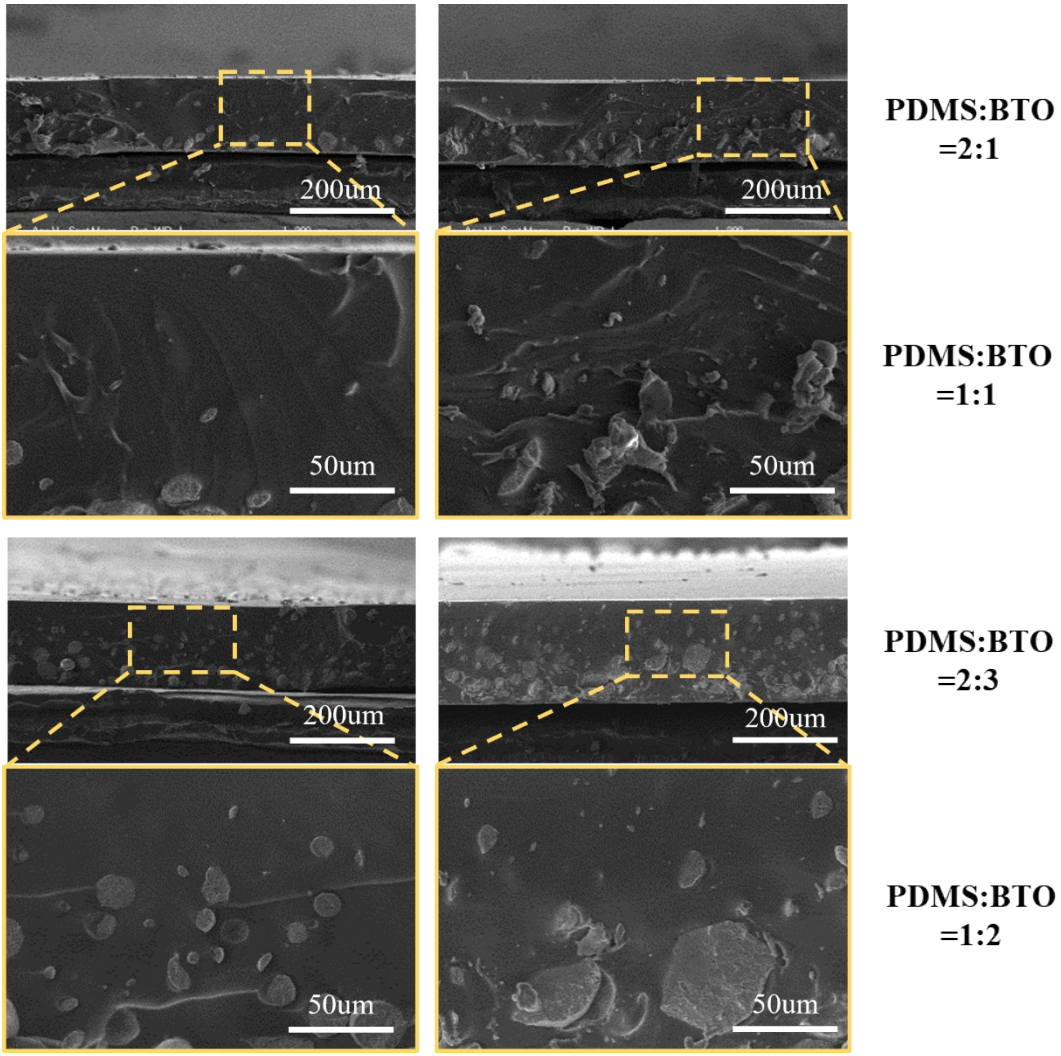

Figure S4 SEM images of PDMS/$BaTiO_3$ based TSL with different doping ratios of 2:1, 1:1, 2:3 and 1:2.

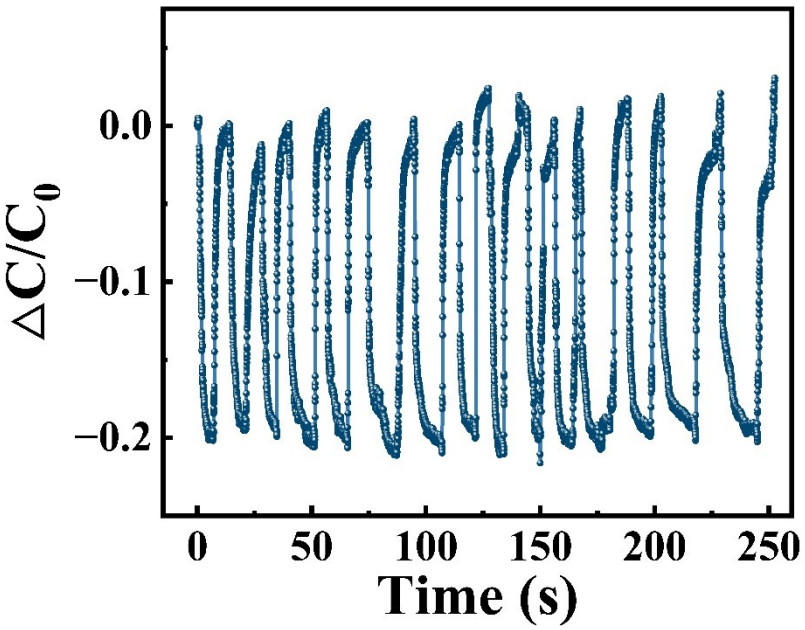

Figure S5 Capacitance variations curve when TSL quickly contacts a 150℃ heat source and a 5℃ cold source.

Table S1: Comparison of our TSL's performance with previously reported capacitive temperature sensors.

Material	Temperature Range	Sensitivity	Linearity	References
Si/Au	20 ℃ ~ 100 ℃	14 fF/℃	No	31
Si/Au bimorph	20 ℃ ~ 100 ℃	15 fF/℃	No	32
Silicon	-70 ℃ ~ 100 ℃	7 fF/℃	Yes	33
Graphene oxide	-70 ℃ ~ 40 ℃	——	No	34
Polysilicon	0 ℃ ~ 100 ℃	32.45 fF/℃	No	35
PDMS	20 ℃ ~ 200 ℃	156 fF/℃	Yes	36
PDMS/$BaTiO_3$	20 ℃ ~ 200 ℃	160.90 fF/℃	Yes	this work

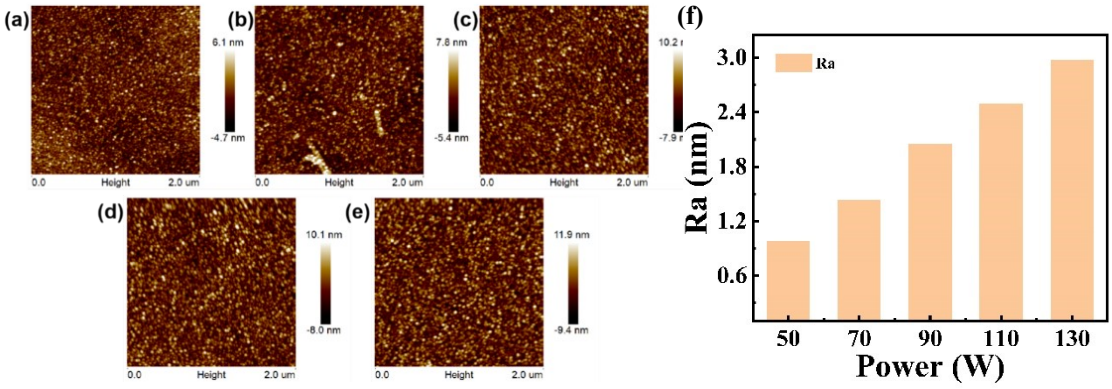

Figure S6: AFM images of Ni80Cr20 thin film obtained at different sputtering powers. At sputtering power of 50W, 70W, 90W, 110W, and 130 W, the corresponding roughness values obtained are 0.978, 1.43, 2.05, 2.49, and 2.97 nm, respectively.

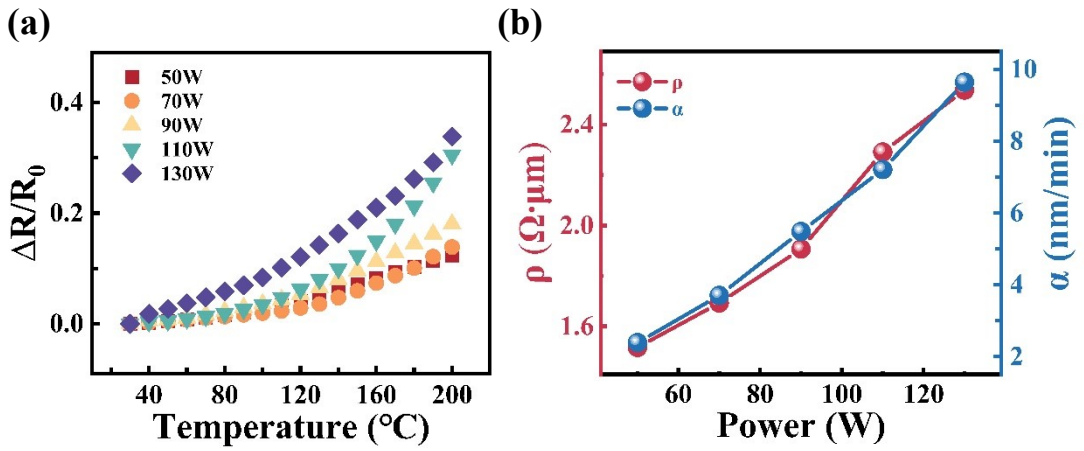

Figure S7: The effect of sputtering power on the electrical properties of SSL: (a)ΔR/R of the sample with temperature at different powers; (b)SSL resistivity and growth rate as a function of sputtering power.

Table S2: Resistivity values obtained at different sputtering powers.

Sputtering power (W)	**50**	**70**	**90**	**110**	**130**
Resistivity（Ω·μm）	**1.51686**	**1.69307**	**1.90675**	**2.29134**	**2.53704**

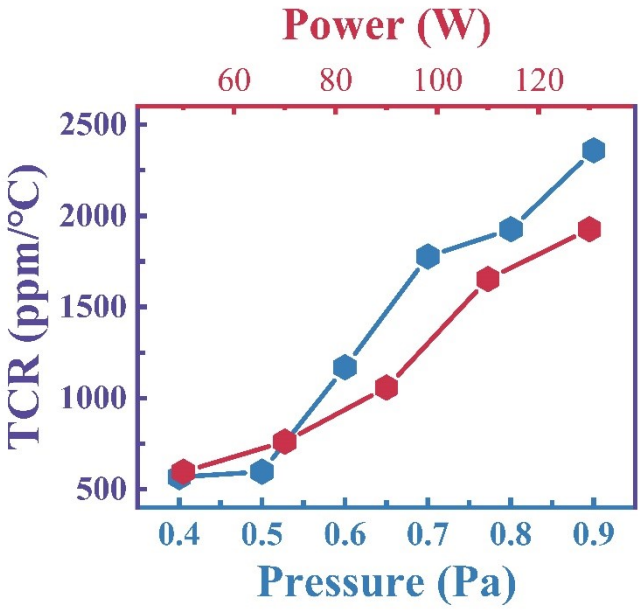

Figure S8: Correlation between TCR, sputtering power and sputtering pressure.

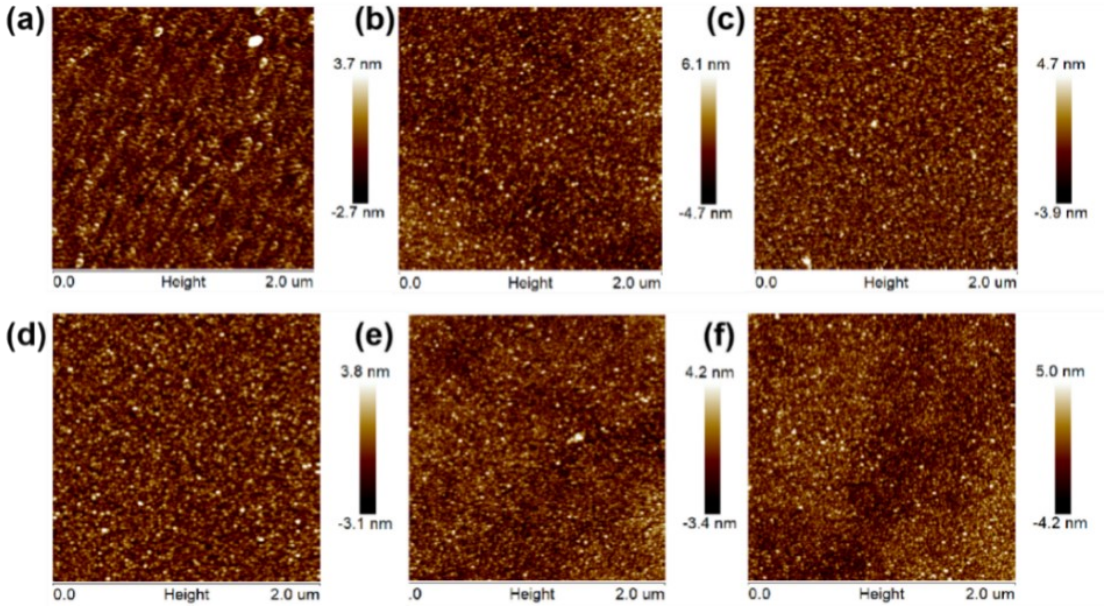

Figure S9: AFM images of Ni80Cr20 film obtained at various sputtering pressure values. Roughness values of 0.904, 0.978, 1.21, 1.64, 2.03 and 2.44 nm are obtained at various sputtering pressures of 0.4, 0.5, 0.6, 0.7, 0.8, and 0.9 Pa, respectively.

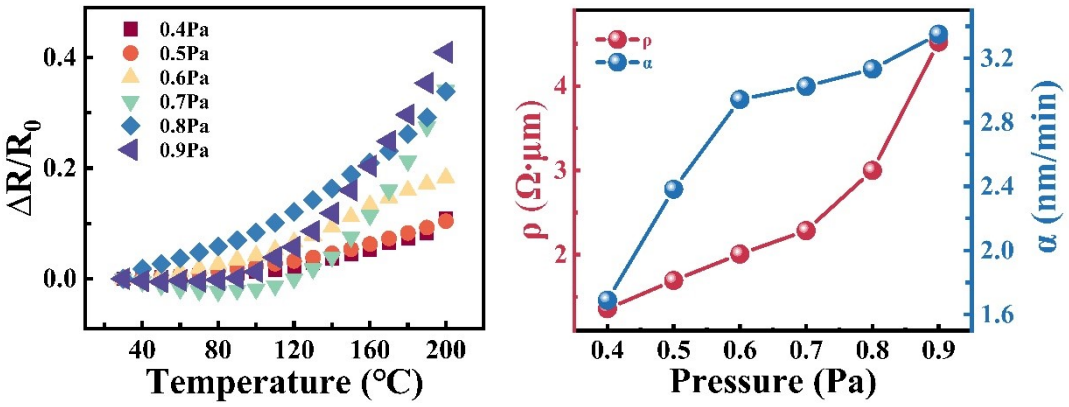

Figure S10: The effect of sputtering pressure on the electrical properties of SSL: (a) ΔR/R of the sample with temperature at different pressures; (b)SSL resistivity and growth rate as a function of sputtering pressure.

Table S3: Resistivity values obtained at different sputtering pressures.

Sputtering pressure (Pa)	**0.4**	**0.5**	**0.6**	**0.7**	**0.8**	**0.9**
Resistivity（Ω·μm）	**1.35767**	**1.51686**	**2.00666**	**2.28497**	**2.99796**	**4.52065**

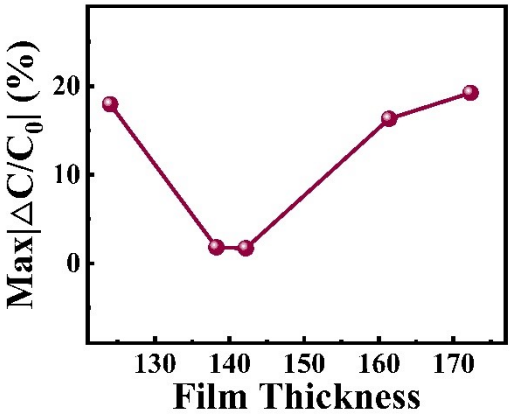

Figure S11: Relation between capacitance value and film thickness during bending.

Table S4: Comparison of our SSL's performance with previously reported strain sensors.

Material	Strain detect limit	response time	References
V-groove mold	0.1 %	130 ms	37
Multilayer graphere	0.4 %	90 ms	38
$Ti_3C_2T_x$ MXene	0.1 %	200 ms	39
KCl/hydrogel	0.05 %	147 ms	40
$Ti_3C_2T_x$ MXene	0.025 %	130 ms	41
Ag	0.01 %	87 ms	42
PDA-GO/CNT-COOH	0.2 %	300 ms	43
Ni80Cr20	0.002 %	54 ms	This work

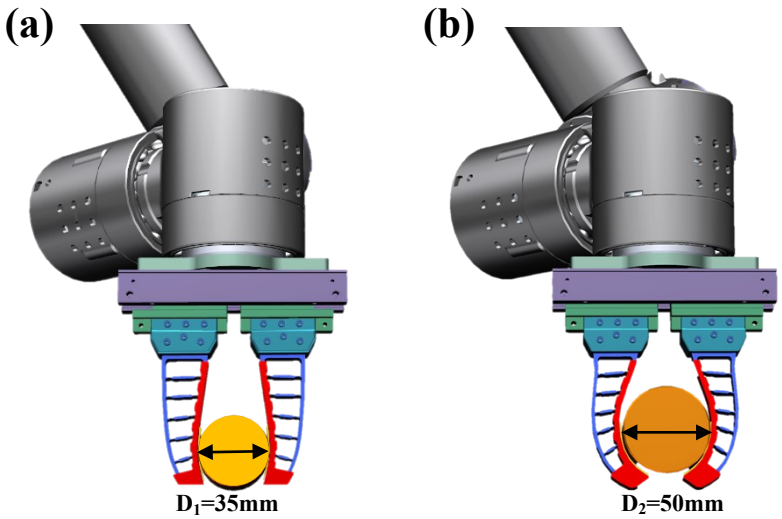

Figure S12: Schematic showing our bimodal sensor incorporated soft gripper to grasp different sized cylinders.

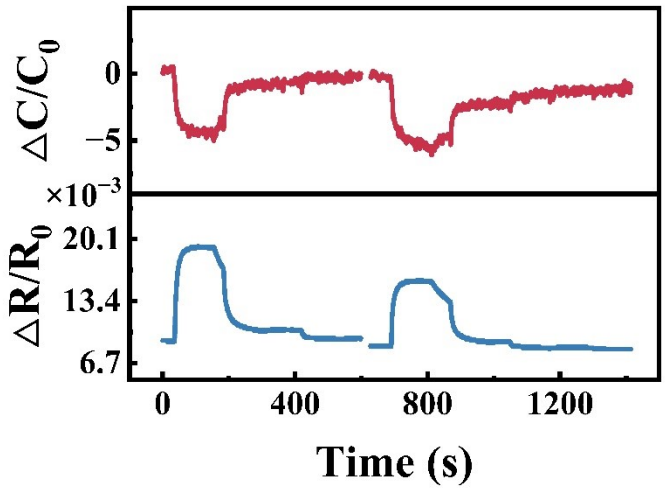

Figure S13: The resultant capacitance and resistance variations, obtained when bimodal sensor incorporated soft gripper is used to grasp different sized cylinders. This confirms that our sensor is fully capable to independently monitor temperature and strain.

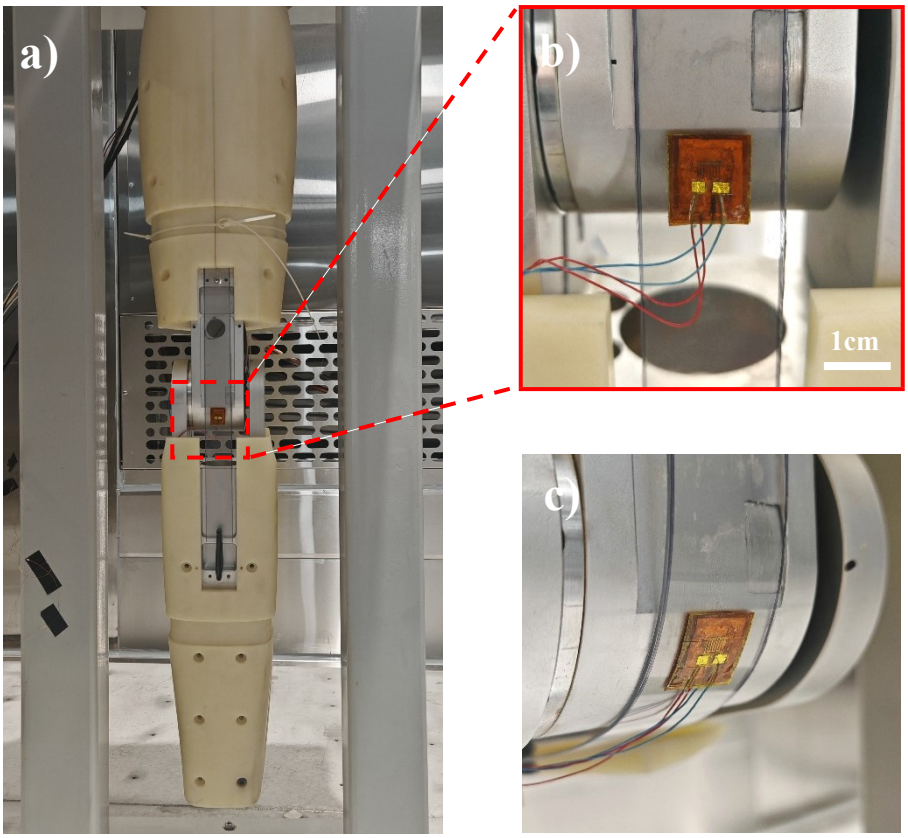

Figure S14 a) Figure showing bimodal sensor incorporated robotic leg, placed in high and low temperature damp heat test chamber; b) Enlarged view of the dual-modal sensor; c) Figure showing sensor incorporated robotic leg under high temperature and bending condition.

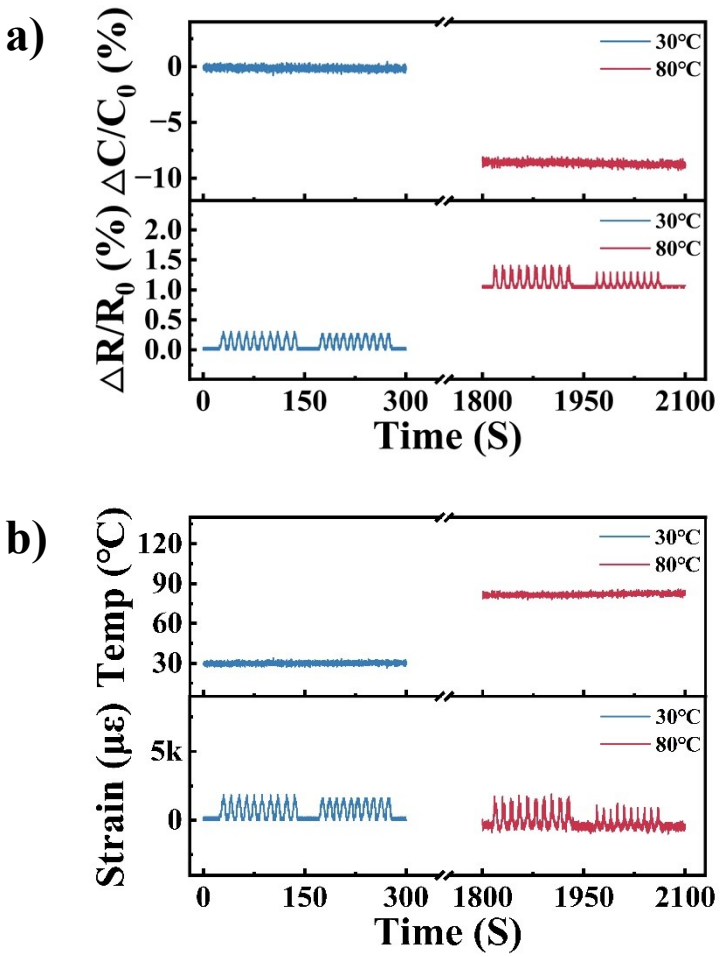

Figure S15 a) Capacitance and resistance curves of our sensor, obtained when the robotic knee is bent at 30° and 20° angles, and at 30°C and 80°C temperature; b) Corresponding temperature and strain magnitude obtained by our proposed decoupling the formula.

According to the capacitance formula：

$$C = \frac{\varepsilon_0 \cdot \varepsilon_{PDMS/BTO} \cdot s}{d_{PDMS/BTO}} = \frac{\varepsilon_0 \cdot \varepsilon_{PDMS/BTO}(T) \cdot w \cdot l}{d_{PDMS/BTO}(T)} \quad (1\text{-}1)$$

where ε_0 represents the vacuum permittivity (≈ 8.854×10^{-12}); $\varepsilon_{(PDMS/BaTO)}$ *is* the relative permittivity of PDMS/$BaTiO_3$; *S* is the electrode area; $d_{PDMS/BaTO}$ is the thickness of the PDMS/$BaTiO_3$ layer; *w* and *l* are the length and width of the electrodes.

The dielectric constant of the PDMS/$BaTiO_3$ temperature-sensitive layer varies with temperature, as shown in the following formula:

$$\varepsilon_{PDMS/BTO}(T) = 32.7 - 0.09625T \quad (1\text{-}2)$$

The expansion formula of the thickness of the PDMS/$BaTiO_3$ temperature-sensitive layer with temperature is shown in the following formula:

$$d_{PDMS/BTO}(T) = d^0{}_{PDMS/BTO}(1 + \alpha_{PDMS/BTO}T)$$

$$= d^0{}_{PDMS/BTO}\left(1 + \frac{\gamma_{PDMS/BTO}}{3}T\right) \quad (1\text{-}3)$$

where $d^0{}_{PDMS/BTO}$ is the initial thickness of the PDMS/$BaTiO_3$ thermosensitive layer, $\alpha_{PDMS/BTO(T)}$ and $\gamma_{PDMS/BTO(T)}$ are the linear expansion coefficient and volume expansion coefficient, respectively.

The empirical relationship between $\gamma_{PDMS/BTO}$ and temperature *T* is shown in the following formula:

$$\gamma_{PDMS\,/\,BTO}(deg^{-1}) = 0.900 * 10^{-3} + 2.76 * 10^{-7}T + 1 * 10^{-10}T^2 \quad (1\text{-}4)$$

Substituting formulas (1-2), (1-3), and (1-4) into formula (1-1),

$$C = \frac{\varepsilon_0 \cdot (32.7 - 0.09625T) \cdot w \cdot l}{d^0{}_{PDMS/BTO} \cdot \left(1 + \frac{\gamma_{PDMS/BTO}}{3}T\right)}$$

When the temperature *T* increases, the dielectric constant $\varepsilon_{PDMS/BTO(T)}$ of the PDMS/$BaTiO_3$ filmdecreases; the volume expansion coefficient of the PDMS/$BaTiO_3$ film $\gamma_{PDMS/BTO(T)}$ increases; the capacitance *C* decreases.

When the environmental temperature remains constant and the deformation in the strain sensor is denoted as ε, the relationship between *Rε* and *ε* can be expressed as:

$$R_\varepsilon = R_0 \times GF \times \varepsilon + R_0 \quad (2\text{-}1)$$

Where R_0 is the initial resistance, *GF* is the sensitivity, and *ε* is the strain.

When there is no deformation applied to the device and only a change in environmental temperature, the relationship between R_T (resistance at temperature T) and temperature T can be expressed as:

$$R_T = R_0\left[1 + TCR\left(T - T_0\right)\right] \quad (2\text{-}2)$$

Where TCR is the temperature coefficient of resistance, and T is temperature, R_0 is the initial resistance, T_0 is the initial temperature.

When the device undergoes deformation and the environmental temperature changes, according to equations (2-1) and (2-2), the resistance R can be expressed as:

$$R = R_0 \times GF \times \varepsilon + TCR(T - T_0)R_0 + R_0 \quad (2\text{-}3)$$